

Characterization of the atmosphere vertical distribution from short-exposures images.

O. Beltramo-Martin^{a,b}, N.A Bharmal^c, C.M. Correia^{d,b}, and T. Fusco^{a,b}

^aONERA, The French Aerospace Laboratory, Marseille, France

^bAix Marseille Univ., CNRS, CNES LAM, Marseille, France

^cCentre for Advanced Instrumentation (CfAI), Durham University, South Road, Durham, DH1 3LE, United Kingdom

^dW. M. Keck Observatory, 65-1120 Mamalahoa Hwy, Kamuela, HI 96743

ABSTRACT

We present PEPITO as a new low-cost and low-complexity concept for profiling the vertical distribution of atmospheric turbulence. PEPITO utilizes *post facto* tip-tilt (TT) corrected short-exposure images to reproduce the anisokinetic effect and then produces the profile estimation using a model-fitting algorithm. We present in this proceedings the methodology we use to estimate the profile and simulation results, that show that PEPITO can reach potentially 1% of accuracy on a 0.5 m telescope by using 5 stars of magnitude $m_V=15$ mag and distributed over a field of 10, arcmin. We present the sensitivity of PEPITO as well as a sky coverage analysis.

Keywords: Atmospheric turbulence

1. INTRODUCTION

Atmospheric characterization for a ground-based telescope has become a key step in the design of instrumentation to correct for wave-front aberrations introduced by atmospheric turbulence. Adaptive Optics (AO) compensates the wave-front aberrations in real-time and the benefits gained from knowledge of the atmospheric profile, or $C_n^2(h)$, include operating the tomographic turbulence compensation in wide-field using multiple Guide Stars (GS),¹⁻⁴ enabling phase predictive control⁵⁻¹⁰ for optimum AO performance, or providing a comprehensive analysis of AO residuals.^{11,12} High altitude layers play a major role in the spatial phase decorrelation¹³ and has an impact on wide-field AO performance¹⁴ and extreme AO.¹⁵ This calls for a high-accuracy, high-altitude profile identification technique.

At present, profiling using AO instruments is performed from the cross-correlation of Wave-Front Sensor (WFS) measurements,^{4,16-20} with profile height limits of $\sim 10-20$ km imposed principally by the telescope diameter, and then additionally the cone effect for laser-based AO.²¹ However, such an approach is only available on multiple GS-based systems and can not be deployed to predict PSF variations on images delivered by single-conjugated AO systems. To achieve this prediction, we must rely on dedicated standalone profilers, such as Stereo-Scidar,²² MASS/DIMM,²³ FASS²⁴ or SLODAR²⁵ instruments, or use predictive weather model.^{26,27}

For PSF modeling purpose, the relevant metric is the focal-plane image, calling for a new type of image-based technique that is capable of retrieving the atmospheric profile from the image itself and not from information of a different nature. In this context, we have proposed the Focal Plane Profiling (FPP) algorithm²⁸ to retrieve the atmospheric profile from the anisoplanatism-affected images through fitting PSF models²⁹ across various points in the field of view (FOV). The use of the focal-plane image is particularly relevant to calibrate the anisoplanatism model regarding the key metric that is the PSF, which can feed algorithms of deconvolution or model-fitting. This technique has revealed to be efficient but needs post-AO images of point sources to be operable, which limits its range of applicability regarding the presence of a sufficient number of bright stars in the field.

Further author information: olivier.beltramo-martin@lam.fr

To keep the strength of a FPP-like approach but make it independent to the AO system, we propose in this paper a novel atmospheric profiling concept, named PEPITO, which uses on-axis Tip-tilt (TT) corrected focal-plane images. PEPITO relies on the TT-anisoplanatism effect³⁰ (commonly called anisokinetism) which elongates the off-axis Point Spread Function (PSF) with respect to the $C_n^2(h)$ profile. This anisoplanatism is created either digitally (*post facto*) from short exposure images (1-10 ms) or by a real-time compensation using a dedicated device. Therefore, we create anisokinetism-contaminated PSFs, without need of AO, which are passed to the FPP algorithm to characterize the atmosphere vertical distribution.

Whereas PEPITO operates from long-exposure focal plane images, therefore using the entire pupil as an aperture, cross-correlation methods instead utilize sub-apertures and then from across all either their centroids (SLODAR) or their scintillation (SCIDAR) is correlated. Consequently, for a given telescope aperture, PEPITO benefits from a full aperture gain³¹ that provides a better signal-to-noise ratio (S/N) for retrieving atmosphere statistics ($C_n^2(h) L_0(h)$).

Each stellar image is spread across a number of detector pixels and there are two important characteristics to consider: the separation from the reference star (baseline) and the change in image (morphology). The baseline gives access to the decorrelation in angle and this is most sensitive for a certain altitude range. The presence of a turbulent layer elongates the PSF in the reference star direction, making the aspect ratio maximal for a baseline value that decrease with respect to the layer height. The morphology encodes the $C_n^2(h)$ and $L_0(h)$ for that altitude range. The range of baselines and the FOV then constrains the altitude limit. The cross-correlation methods have fundamentally a baseline-equivalent angular separation of two stars together with spacings of the sub-apertures in the pupil, from their widths to the diameter of the pupil. The angular separation and sub-aperture size or pupil diameter determines, respectively, the altitude spacing of the profile and the upper altitude limit. Therefore despite both methods reliance on the angular decorrelation of phase from atmospheric turbulence, and for PEPITO and SLODAR specifically the TT component, the resulting characteristics favour PEPITO for high-resolution profiling at better than few hundreds of meters. Finally, PEPITO relies on long-exposure PSFs that have statistically converged, i.e. their aspect ratio and Full Width at Half Maximum (FWHM) does not vary by accumulating more frames, which can be reached in tens of seconds to one minute regarding the seeing conditions. This implies a temporal resolution improvement by $5 \times$ compared to existing methods that commonly provide profiles at the rate of 2 up to 5 minutes.²²

2. CONCEPT

With PEPITO, we firstly aim at reproducing the anisoplanatism effect that occurs in wide-field AO-assisted images, but without any AO system, from which we will be able to use the FPP technique to estimate the $C_n^2(h)$. A straightforward solution consists in compensating the tip-tilt modes only, either digitally from short-exposure images, or using a dedicated tip-tilt compensation mirror. We concentrate our analysis on the first solution that has the benefit to rely on the simplest hardware implementation: a telescope plus a fast readable camera. We report in Fig. 2 an illustration of digital anisokinetism-corrected PSFs as function of the separation from the reference stars tip-tilt modes are measured on.

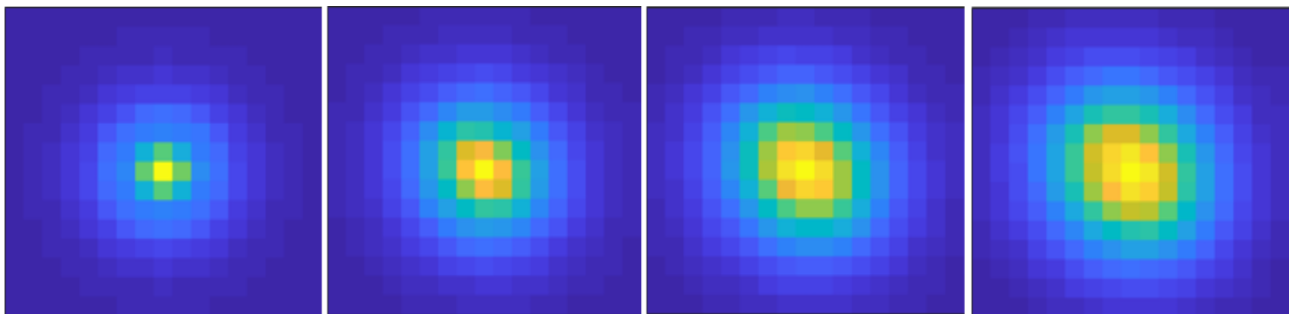


Figure 1. Illustration of the impact of anisokinetism on long-exposure PSFs at different separation from the the tip-tilt star. **Left to right:** 0, 15, 30 and 45 arcsec. The intensity scale changes to enhance the contrast on the PSF elongation.

Equations and detailed methodology is described in,³² we remind here the main steps.

1. **Acquire short exposures images (10-50 ms).** We need a large field of view, potentially up to 5 up to 10 arcmin, which is achievable with a 2k×2k camera and a pixel scale of 250 to 500 mas. Accounting for 30s of exposure, we need $n_{\text{exp}} = 600$ up to 3,000 frames.
2. **Extract the n_{stars} imaged PSFs distributed over the field.** Thanks to the large pixel scale, handling small sub-images of 20×20 pixels is reasonably large enough to capture the anisoplanatism signature.
3. **Stack PSFs cubes across the n_{exp} frames.** We end up having n_{stars} long-exposure images on which we can estimate the seeing, global outer scale and potentially the residual jitter due to instrumental effects (vibrations due to telescope tracking for instance). We may use the approach proposed by³³ by modeling the PSF from the Von-Kärmmann atmospheric phase Power Spectrum Density (PSD)¹³ and convolving the obtained PSF with an asymmetric Gaussian. The atmospheric PSD will depend on the seeing and the outer scale, while the Gaussian PSF is a function of two parameters (PSF FWHM in x and y). With this model, we can perform a joint-estimation of those four parameters using the n_{stars} PSFs.
4. **Introduce the digital anisokinetism by choosing a reference stars among the n_{stars} sources.** One must measure the tip-tilt modes from the corresponding PSF frame-by-frame (herein we do estimate it from the PSF barycenter), compensate each of the n_{stars} from this signal and stack across time. Because the spatial decorrelation of tip-tilt modes, stars away from the reference PSF will be partially corrected and contaminated by the anisokinetism effect as illustrated in Fig. 2. This step is therefore done n_{stars} times by changing the reference stars to obtain eventually $n_{\text{stars}} \times (n_{\text{stars}} - 1)$ long-exposure PSFs. Actually, there are only $n_{\text{stars}} \times (n_{\text{stars}} - 1)/2$ non-redundant couples; however each PSF is affected differently by telescope static aberrations, advocating for including redundant measurements to mitigate non-atmospheric effects that modify the PSF morphology.
5. **Perform a joint best-fitting over the $n_{\text{stars}} \times (n_{\text{stars}} - 1)$ images to estimate the $C_n^2(h)$.** Refer to²⁸ to get details about the implementation. As a summary, we deploy a non-linear least-square minimization algorithm that will iterate on the $C_n^2(h)$ discretized over n_L layers (altitude, outer scale fixed) to calibrate the PSF model on the ensemble of observations. One may also constrain the solution to get the $C_n^2(h)$ integral from the seeing estimation in step 3.

3. SIMULATION RESULTS

We summarize results presented in.³² A first verification was made on the PSF model accuracy. We report in Fig. 3 the excellent agreement between the end-to-end simulated PSF and the model at $\theta = 16$ arcsec. This is also verified for all positions, with an overall residual lower than 0.2% in worst case, reassuring on our capability to estimate correctly the $C_n^2(h)$ from this technique.

Now, we have played the full PEPITO game by simulated a 7-layers profile and 3,000 short-exposure images 10ms-long each. We report in Fig. 3 the $C_n^2(h)$ estimation error (average over the whole profile) as function of the wind speed value and the star magnitude.

Error drops down 1% for a regime of wind speed from 15 m/s to 30 m/s but increase apart from this scheme. For a lowest turbulence, the $C_n^2(h)$ error increases due to a lack of atmosphere statistics convergence, which can be solved by integrating longer. For higher wind speed values than 30 m/s, the error slightly goes up to 2%, but for a different reason: because the finite exposure time of 10 ms, the tip-tilt estimation becomes less accurate when the atmosphere coherence time get shorter. The time averaging serves as a low-pass filter^{34,35} that blurs the PSF and introduces an additional component that superimposes to the TT-anisoplanatism effect and diminishes the PEPITO sensitivity. However, according to,³⁵ the important scalar parameter to focus on is the atmosphere characteristic time defined as $T_0 = \pi.D/v_{8/3}$, where:

$$v_{8/3} = \left(\frac{\int_0^\infty C_n^2(h)v(h)^{8/3}dh}{\int_0^\infty C_n^2(h)dh} \right)^{3/8}. \quad (1)$$

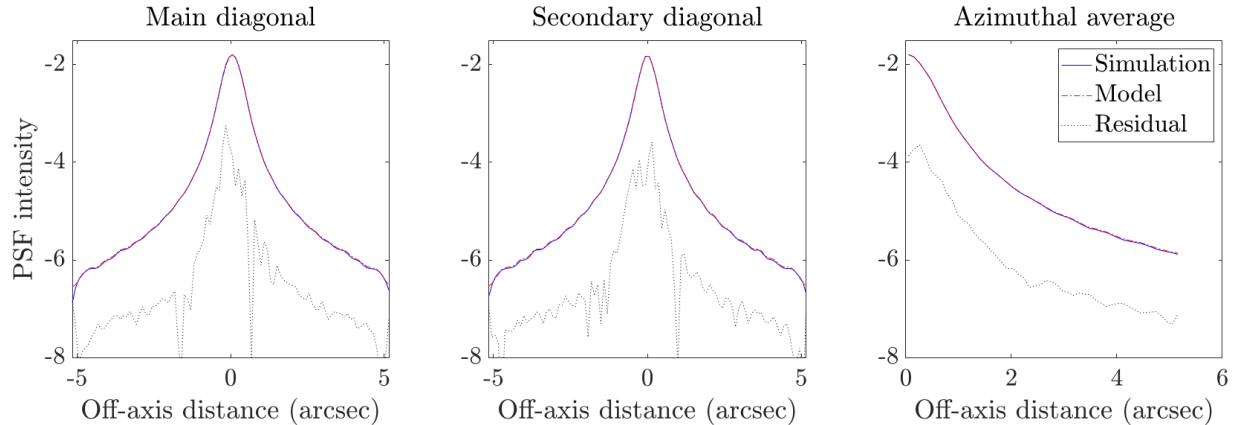


Figure 2. Comparison of simulated and analytical anisoplanatic PSFs. Simulations were produced with OOMAO.

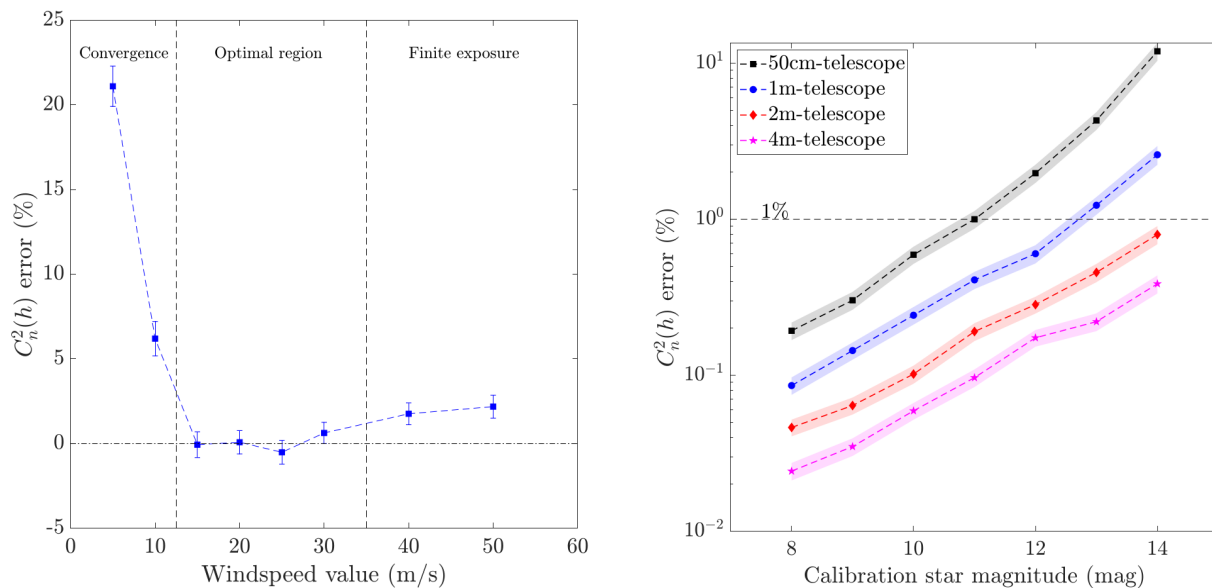


Figure 3. Relative estimation error on the $C_n^2(h)$ using a single star as function of **Left:** the simulated windspeed value **Right:** the star magnitude.

For a 1m-telescope and with $T = 10\text{ms}$ as the exposure time, we get $T/T_0 = 0.1$ for respectively a wind speed value of 30 m/s, which correspond to the limit presented by³⁵ to consider the finite exposure time as negligible in the seeing estimation. It coincides with our present results showing the estimates accuracy degradation up to 2% for faster wind speed than 30 m/s. According to recent surveying of the atmospheric profile at Paranal,^{22,36} having a layer that combines high speed ($> 30\text{ m/s}$) and large strength ($> 5\%$ of the whole profile) as well as high altitude ($> 10\text{ km}$) to produce a detectable anisoplanatism signature is not frequent, advocating for a mitigation of this effect with PEPITO, especially regarding the convergence issue that is the main constrain that will specify the exposure time.

Fig. 3 gives also the $C_n^2(h)$ error with respect to the star magnitude for different telescope sizes. We notice that 1% of accuracy can be reached on a 0.5 m telescope by relying on a single star of $m_V = 11$, with a pixel scale of 500 mas and a narrow spectral filter of 10 nm. In a more realistic scenario, we must have $n_{\text{stars}} > 1$ (5-stars

asterisms have been found observable at La Palma for instance) and a wider spectral band. Because atmospheric chromatism effect, we should probably limit the filter band to 50 nm . Eventually, with this configuration, PEPITO will reach few percent of error by handling 5 stars with $mV = 15$.

4. SENSITIVITY AND RESOLUTION

Any tip-tilt compensated long-exposure PSF is affected by the whole $C_n^2(h)$ distribution. However, the signature of a particular layer is maximal for a specific angular separation, e.g. it produces a maximal anisokinetism effect. This is illustrated in Fig. 4 where we report the PSF aspect ratio as function of the off-axis distance from the reference star and for a sole-layer profile with various layer heights. We notice that lowest layer produce a maximal signature at farthest separation. Indeed, to create the anisokinetism effect, we need to have a partial decorrelation of tip-tilt modes, which is controlled by the product $h \times \theta$, where h is the layer height. If $h \times \theta$ is too small, there is a strong spatial correlation that does not bring enough diversity to differentiate off-axis PSFs from the reference PSF, e.g. the PSF elongation due to the anisokinetism is too small regarding the reference PSF FWHM. On the contrary, if there is a total decorrelation, the off-axis PSF becomes circular and no $C_n^2(h)$ estimation is possible.

As a summary, each baseline in the focal-plane permits to estimate one of several layers located a particular range of altitude, that depends on the telescope diameter D , the separation θ and the anisokinetism angle θ_a that controls the tip-tilt decorrelation rate. Therefore, for n_{stars} , we may retrieve at least $n_{\text{stars}} \times (n_{\text{stars}} - 1)/2$.

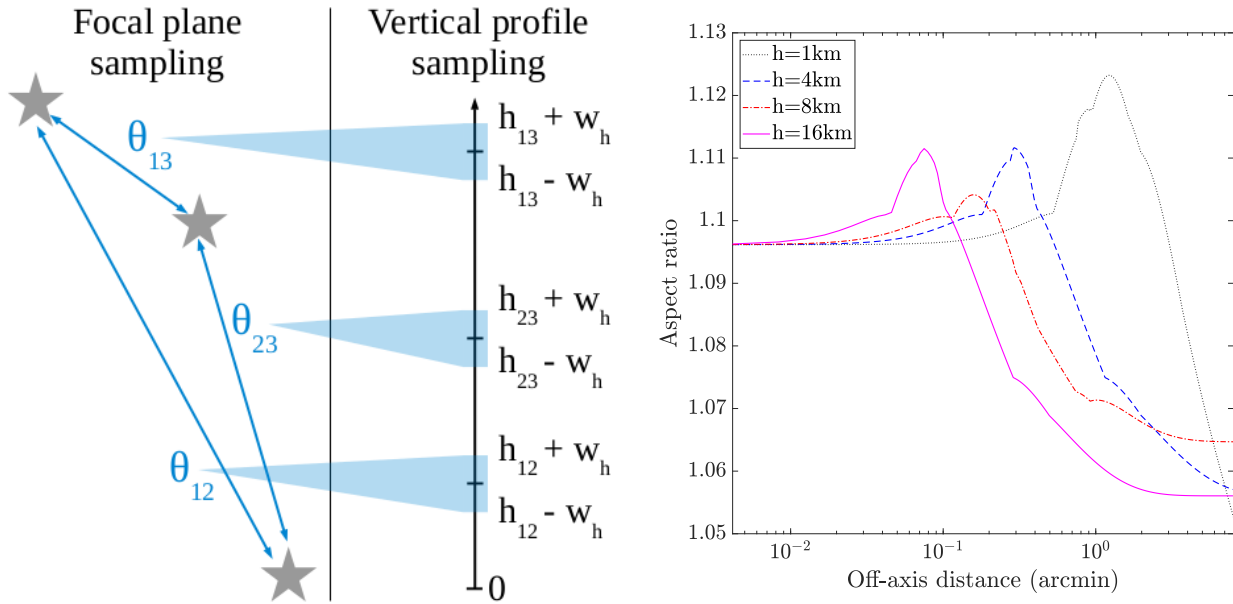


Figure 4. Illustration of the possible baselines by choosing each star in turn as the reference. Each baseline permits the estimation of the atmospheric profile at specific height range whose the width w_h . In practice, each baseline has a second, redundant but independent measurement when the reference star and the anisokinetically affected star switch place e.g. $h_{12} \equiv h_{21}$. Evolution of the PSF aspect ratio as function of the separation and resolution wrt the layer height.

We indicate in Fig. 4 the altitude resolution with respect to the layer height and the pixel scale $\Delta\theta$ as well as the telescope Field of view (FOV) we need regarding the height of the layer we want to characterize. The altitude resolution increases with respect to h^2 and decreases with smaller pixel scales. This is due to the fact that the FOV decreases rapidly with h , which causes a confusion between high-altitude layers. For instance, with a 0.5 m telescope, two layers at 16 and 20 km provokes a maximal anisokinetism at respectively $\theta = 5.4$ and 4.4 arcsec. With 500 mas of resolution, this corresponds to a difference of 2 pixels only. This can be improved by diminishing the pixel scale or increase the telescope size, but larger format camera is therefore required. There

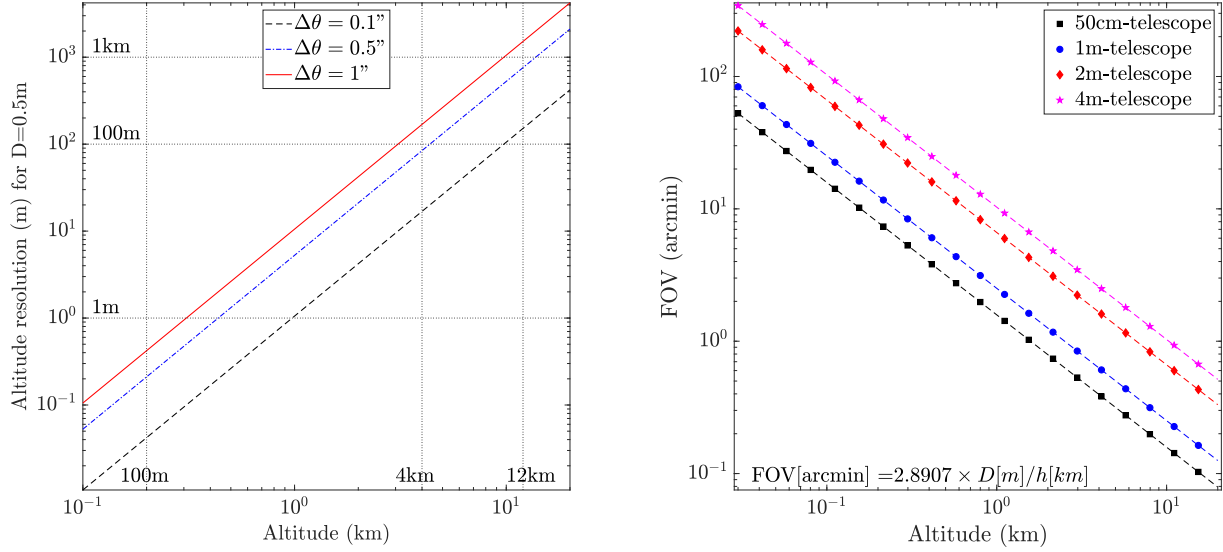


Figure 5. PEPITO altitude resolution with respect to the layer height for various pixel scale values $\Delta\theta$.

is a trade-off on the telescope size, pixel scale and exposure to optimize the PEPITO accuracy regarding the asterism geometry.

5. SKY COVERAGE

Regarding that we need at least five stars of magnitude $mV=15$ to obtain a proper $C_n^2(h)$ estimation, one may estimate the sky coverage of PEPITO. The probability density of a baseline with length θ given m stars within the field of radius Θ is written as $\mathcal{P}_B(\theta; m, \Theta)$. Because stars are assumed isotropically and randomly distributed within Θ , their number density, ρ_* , is also constant within Θ . Then that leads to the expected number of stars being $m_{\rho_*} = \pi\Theta^2\rho_*$. The consequence is that \mathcal{P}_B only depends on the overlap of the field at the baseline length θ and the probability of having m stars $\mathcal{P}_m(m; m_{\rho_*})$ as follows

$$\mathcal{P}_B(\theta; m, \Theta) = \left(2\Theta^2 \arccos\left(\frac{\theta}{2\Theta}\right) - \frac{\theta}{2} \sqrt{4\Theta^2 - \theta^2} \right) \frac{1}{\pi^2 \Theta^4} \mathcal{P}_m(m; m_{\rho_*}) \quad (2)$$

The probability of m stars (rather than assuming a fixed m_{ρ_*}) is a Poisson distribution with expectation m_{ρ_*} , and variance m as

$$\mathcal{P}_m(m, m_{\rho_*}) = \frac{m_{\rho_*}^m e^{-m_{\rho_*}}}{m!} = \exp(m \log m_{\rho_*} - m_{\rho_*} - \log \Gamma(m + 1)). \quad (3)$$

which allows to obtain the expectation of having a baseline of length θ with range Δ

$$\mathbb{E}(\mathcal{B}; \theta, \Delta) = 2\pi \sum_{m=m_{\min}}^{\infty} m(m-1) \int_{\theta-\Delta}^{\theta+\Delta} \mathcal{P}_B(\theta; m, \Theta) \theta d\theta. \quad (4)$$

Eventually, from the averaged stellar density per square degree, one may derive $\mathbb{E}(\mathcal{B}; \theta, \Delta)$ for any wished baseline. The sky coverage is then deduced by the multiplication of probability functions and is reported in Tab. 1 as function of the Galactic zenith angle. Actually, the sky coverage reaches 1% at the Galactic poles, which is very low but sufficient for having a suitable asterism for atmospheric profiling.

Table 1. Sky coverage estimation for finding an asterism containing 5 baseline with $mV < 15$.

θ range (arcsec)	Value of $\mathbb{E}(\mathcal{B}; \theta, \Delta)$ for $mV=15$ mag	
	90° ZA	20° ZA
323.0 ± 10.0	0.937	0.996
142.0 ± 10.0	0.753	0.942
74.0 ± 10.0	0.534	0.79
23.0 ± 10.0	0.219	0.396
8.8 ± 8.8	0.0812	0.159
Sky coverage	1%	5%

6. CONCLUSION

We have presented PEPITO as a new concept of atmospheric turbulence profiling based on wide-field, short-exposure images in seeing-limited mode. It involves a simplest hardware implementation made of a small telescope (0.3-1 m) and a fast readable (10-50 ms) and large format (2k×2k) camera. PEPITO reproduces the anisokinetic effect by compensating the tip-tilt frame-by-frame according to the reference PSF barycenter. Therefore, PEPITO inverses the problem to retrieve the $C_n^2(h)$ that produces the elongation of observed long-exposure PSFs distributed across the field.

We have summarized the steps followed by PEPITO to obtain the $C_n^2(h)$ from the cube of short exposure images. We have validated the concept using end-to-end simulations and illustrated that PEPITO can limit the estimation error down to 1% by using 5 stars of magnitude $mV < 15$ with a pixel scale of 250-500 mas.

Next steps will consist in processing data acquired at La Palma in July 2019 and measure the seeing and the $C_n^2(h)$ with PEPITO, to be compared with SCIDAR measurements.

ACKNOWLEDGMENTS

This work was supported by the A*MIDEX project (no. ANR-11-IDEX-0001-02) funded by the "Investissements d'Avenir" French Government programme, managed by the French National Research Agency (ANR). This work is also supported OPTICON H2020 WP10. NAB acknowledges UKRI STFC funding (ST/P000541/1).

REFERENCES

- [1] Ono, Y. H., Correia, C., Conan, R., Blanco, L., Neichel, B., and Fusco, T., "Fast iterative tomographic wavefront estimation with recursive Toeplitz reconstructor structure for large-scale systems," *Journal of the Optical Society of America A* **35**, 1330 (Aug. 2018).
- [2] Ono, Y. H., Akiyama, M., Oya, S., Lardi re, O., Andersen, D. R., Correia, C., Jackson, K., and Bradley, C., "Multi time-step wavefront reconstruction for tomographic adaptive-optics systems," *JOSAA* **33**, 726 (Apr. 2016).
- [3] Correia, C. M., Jackson, K., V eran, J.-P., Andersen, D., Lardi re, O., and Bradley, C., "Spatio-angular minimum-variance tomographic controller for multi-object adaptive-optics systems," *Applied Optics* **54**, 5281 (June 2015).
- [4] Vidal, F., Gendron, E., and Rousset, G., "Tomography approach for multi-object adaptive optics," *JOSA A* **27**, A253–A264 (Nov. 2010).
- [5] Correia, C. M., Bond, C. Z., Sauvage, J.-F., Fusco, T., Conan, R., and Wizinowich, P. L., "Modeling astronomical adaptive optics performance with temporally filtered Wiener reconstruction of slope data," *Journal of the Optical Society of America A* **34**, 1877 (Oct. 2017).
- [6] Males, J. R. and Guyon, O., "Ground-based adaptive optics coronagraphic performance under closed-loop predictive control," *Journal of Astronomical Telescopes, Instruments, and Systems* **4**, 019001 (Jan. 2018).
- [7] Juv enal, R., Kulcs ar, C., Raynaud, H.-F., and Conan, J.-M., "LQG adaptive optics control with wind-dependent turbulent models," in *[Adaptive Optics Systems V]*, *Proc. SPIE* **9909**, 99090M (July 2016).

- [8] Sivo, G., Kulcsár, C., Conan, J.-M., Raynaud, H.-F., Gendron, É., Basden, A., Gratadour, D., Morris, T., Petit, C., Meimon, S., Rousset, G., Garrel, V., Neichel, B., van Dam, M., Marin, E., Carrasco, R., Schirmer, M., Rambold, W., Moreno, C., Montes, V., Hardie, K., and Trujillo, C., “On-sky validation of an optimal LQG control with vibration mitigation: from the CANARY Multi-Object Adaptive Optics demonstrator to the Gemini Multi-Conjugated Adaptive Optics facility,” in [*American Astronomical Society Meeting Abstracts*], *American Astronomical Society Meeting Abstracts* **225**, 413.07 (jan 2015).
- [9] Rudy, A. R., Srinath, S., Poyneer, L., Ammons, S. M., Gavel, D., Kupke, R., Dillon, D., and Rockosi, C., “Progress towards wind predictive control on ShaneAO: test bench results,” in [*Adaptive Optics Systems IV*], *Proc. SPIE* **9148**, 91481Z (July 2014).
- [10] Petit, C., Sauvage, J.-F., Fusco, T., Sevin, A., Suarez, M., Costille, A., Vigan, A., Soenke, C., Perret, D., Rochat, S., Barufolo, A., Salasnich, B., Beuzit, J.-L., Dohlen, K., Mouillet, D., Puget, P., Wildi, F., Kasper, M., Conan, J.-M., Kulcsár, C., and Raynaud, H.-F., “SPHERE eXtreme AO control scheme: final performance assessment and on sky validation of the first auto-tuned LQG based operational system,” in [*Adaptive Optics Systems IV*], *Proc. SPIE* **9148**, 91480O (Aug. 2014).
- [11] Ferreira, F., Gendron, E., Rousset, G., and Gratadour, D., “Numerical estimation of wavefront error breakdown in adaptive optics,” *Astron. & Astrophys.* **616**, A102 (Aug. 2018).
- [12] Martin, O. A., Gendron, É., Rousset, G., Gratadour, D., Vidal, F., Morris, T. J., Basden, A. G., Myers, R. M., Correia, C. M., and Henry, D., “Wave-front error breakdown in laser guide star multi-object adaptive optics validated on-sky by Canary,” *Astron. & Astrophys.* **598**, A37 (Feb. 2017).
- [13] Roddier, F., “The effects of atmospheric turbulence in optical astronomy,” *Progress in optics. Volume 19. Amsterdam, North-Holland Publishing Co., 1981, p. 281-376.* **19**, 281–376 (1981).
- [14] Costille, A. and Fusco, T., “Impact of Cn² profile on tomographic reconstruction performance: application to E-ELT wide field AO systems,” in [*Adaptive Optics Systems III*], *Proc. SPIE* **8447**, 844757 (July 2012).
- [15] Cantalloube, F., Por, E., Dohlen, K., Sauvage, J.-F., Vigan, A., Kasper, M., Bharmal, N., Henning, T., Brandner, W., Milli, J., Correia, C., and Fusco, T., “Origin of the asymmetry of the wind driven halo observed in high contrast images,” *ArXiv e-prints* (Oct. 2018).
- [16] Laidlaw, D. J., Osborn, J., Morris, T. J., Basden, A. G., Beltramo-Martin, O., Butterley, T., Gendron, E., Reeves, A. P., Rousset, G., Townson, M. J., and Wilson, R. W., “Optimising the accuracy and efficiency of optical turbulence profiling using Adaptive Optics telemetry for Extremely Large Telescopes,” *M.N.R.A.S* , *accepted* (Dec. 2018).
- [17] Mazzoni, T., Busoni, L., Bonaglia, M., and Esposito, S., “Atmospheric turbulence profiling using the SLODAR technique with ARGOS at LBT,” in [*Adaptive Optics Systems V*], *Proc. SPIE* **9909**, 99093R (July 2016).
- [18] Ono, Y. H., Correia, C. M., Andersen, D. R., Lardière, O., Oya, S., Akiyama, M., Jackson, K., and Bradley, C., “Statistics of turbulence parameters at Maunakea using the multiple wavefront sensor data of RAVEN,” *M.N.R.A.S* **465**, 4931–4941 (Mar. 2017).
- [19] Martin, O. A., Correia, C. M., Gendron, E., Rousset, G., Vidal, F., Morris, T. J., Basden, A. G., Myers, R. M., Ono, Y. H., Neichel, B., and Fusco, T., “William Herschel Telescope site characterization using the MOAO pathfinder CANARY on-sky data,” in [*Adaptive Optics V from proc. SPIE*], (2016).
- [20] Neichel, B., Masciadri, E., Guesalaga, A. R., Lascaux, F., and Béchet, C., [*Towards a reliability assessment of the C²_N and wind speed vertical profiles retrieved from GeMS*], vol. 9148 of *Proc. SPIE* , 63 (Aug. 2014).
- [21] Foy, R., “The Cone Effect,” in [*Laser Guide Star Adaptive Optics for Astronomy*], Ageorges, N. and Dainty, C., eds., 107 (2000).
- [22] Osborn, J., Wilson, R. W., Sarazin, M., Butterley, T., Chacón, A., Derie, F., Farley, O. J. D., Haubois, X., Laidlaw, D., LeLouarn, M., Masciadri, E., Milli, J., Navarrete, J., and Townson, M. J., “Optical turbulence profiling with Stereo-SCIDAR for VLT and ELT,” *M.N.R.A.S* **478**, 825–834 (July 2018).
- [23] Butterley, T., Sarazin, M., Navarrete, J., Osborn, J., Farley, O., and Le Louarn, M., “Improvements to MASS turbulence profile estimation at Paranal,” in [*Proc. SPIE*], *Society of Photo-Optical Instrumentation Engineers (SPIE) Conference Series* **10703**, 107036G (Jul 2018).
- [24] Guesalaga, A., Perera, S., Osborn, J., Sarazin, M., Neichel, B., and Wilson, R., “FASS: the full aperture seeing sensor,” in [*Adaptive Optics Systems V*], *Proc. SPIE* **9909**, 99090H (July 2016).

- [25] Wilson, R. W., “SLODAR: measuring optical turbulence altitude with a Shack-Hartmann wavefront sensor,” *M.N.R.A.S* **337**, 103–108 (Nov. 2002).
- [26] Osborn, J. and Sarazin, M., “Atmospheric turbulence forecasting with a general circulation model for Cerro Paranal,” *M.N.R.A.S* **480**, 1278–1299 (Oct. 2018).
- [27] Masciadri, E., Lascaux, F., Turchi, A., and Fini, L., “Optical turbulence forecast: ready for an operational application,” *M.N.R.A.S* **466**, 520–539 (Apr. 2017).
- [28] Beltramo-Martin, O., Correia, C. M., Neichel, B., and Fusco, T., “Focal-plane $C_n^2(h)$ profiling based on single-conjugate adaptive optics compensated images,” *M.N.R.A.S* **481**, 2349–2360 (Dec. 2018).
- [29] Beltramo-Martin, O., Correia, C. M., Mieda, E., Neichel, B., Fusco, T., Witzel, G., Lu, J. R., and Véran, J.-P., “Off-axis point spread function characterization in laser guide star adaptive optics systems,” *M.N.R.A.S* **478**, 4642–4656 (Aug. 2018).
- [30] Fried, D. L., “Anisoplanatism in adaptive optics,” *Journal of the Optical Society of America (1917-1983)* **72**, 52 (Jan. 1982).
- [31] Plantet, C., Meimon, S., Conan, J.-M., and Fusco, T., “Experimental validation of LIFT for estimation of low-order modes in low-flux wavefront sensing,” *Optics Express* **21**, 16337 (July 2013).
- [32] Beltramo-Martin, O., Bharmal, N., and Correia, C. M., “PEPITO: atmospheric Profiling from short-Exposure focal Plane Images in seeing-limited mode,” *M.N.R.A.S*, *submitted* (2018).
- [33] Martinez, P., Kolb, J., Sarazin, M., and Tokovinin, A., “On the Difference between Seeing and Image Quality: When the Turbulence Outer Scale Enters the Game,” *The Messenger* **141**, 5–8 (Sept. 2010).
- [34] Martin, H. M., “Image motion as a measure of seeing quality,” *Publications of the Astronomical Society of the Pacific* **99**, 1360–1370 (Dec. 1987).
- [35] Hickson, P., Ma, B., Shang, Z., and Xue, S., “Multistar turbulence monitor: a new technique to measure optical turbulence profiles,” *M.N.R.A.S* **485**, 2532–2545 (May 2019).
- [36] Masciadri, E., Lombardi, G., and Lascaux, F., “On the comparison between MASS and generalized-SCIDAR techniques,” *M.N.R.A.S* **438**, 983–1004 (Feb. 2014).